

PLATOSpec’s first results: planets WASP-35b and TOI-622b are on aligned orbits, and K2-237b is on a polar orbit

J. Zak¹, P. Kabath¹, H. M. J. Boffin², J. Liptak^{1,3}, M. Skarka¹, R. Brahm^{4,5}, P. Gajdoš^{1,6}, A. Bocchieri⁷, D. Itrich⁸,
L. Vanzì^{9,5}, P. Pintr¹⁰, J. Janik¹¹, and A. Hatzes¹²

¹ Astronomical Institute of the Czech Academy of Sciences, Fričova 298, 25165 Ondřejov, Czech Republic; e-mail: zak@asu.cas.cz

² European Southern Observatory, Karl-Schwarzschild-str. 2, 85748 Garching, Germany

³ Astronomical Institute of Charles University, V Holešovičkách 2, CZ-180 00 Prague, Czech Republic

⁴ School of engineering and sciences, Universidad Adolfo Ibañez, Av. Diag. Las Torres 2640, 7941169 Santiago, Chile

⁵ Center of Astro Engineering, Pontificia Universidad Católica de Chile, Av. Vicuña Mackenna 4860, 782-043 Santiago, Chile

⁶ Institute of Physics, Faculty of Science, Pavol Jozef Šafárik University, Park Angelinum 9, 040 01 Košice, Slovakia

⁷ Dipartimento di Fisica, La Sapienza Università di Roma, Piazzale Aldo Moro 5, Roma, 00185, Italy

⁸ Steward Observatory, The University of Arizona, 933 N. Cherry Ave, Tucson, AZ 85721, USA

⁹ Department of Electrical Engineering, Pontificia Universidad Católica de Chile, Av. Vicuña Mackenna 4860, 782-043 Santiago, Chile

¹⁰ Department of Theoretical Physics and Astrophysics, Masaryk University, Kotlářská 2, 60200 Brno, Czech Republic

¹¹ Institute of Plasma Physics of Czech Academy of Sciences, U Slovanky 2525/1a, 182 00 Praha 8, Czech Republic

¹² Thüringer Landessternwarte, D-07778 Tautenburg, Germany

Received June 28, 2025; accepted August XX, 2025

ABSTRACT

The spin-orbit angle between a stellar spin axis and its planetary orbital axis is a key diagnostic of planetary migration pathways, yet the mechanisms shaping the observed spin-orbit distribution remain incompletely understood. Combining the spin-orbit angle with atmospheric measurements has emerged as a powerful method of studying exoplanets that showcases the synergy between ground- and space-based observations. We present the Rossiter-McLaughlin effect measurements of the projected spin-orbit angle (λ) for three gaseous exoplanets using the newly commissioned PLATOSpec instrument on the E152 Telescope at La Silla Observatory. For WASP-35b, we determine $\lambda = 1^{+19}_{-18}$ deg, demonstrating PLATOSpec’s capabilities through excellent agreement with HARPS-N literature data. We provide the first spin-orbit measurements for TOI-622b ($\lambda = -4 \pm 12$ deg, true spin-orbit angle $\psi = 16.1^{+8.0}_{-9.7}$ deg), revealing an aligned orbit consistent with quiescent disc migration. For K2-237b, we find $\lambda = 91 \pm 7$ deg and $\psi = 90.5^{+6.8}_{-6.2}$ deg, indicating a nearly perfect polar orbit, which suggests a history consistent with disc-free migration, contrasting previous studies inferring disc migration. TOI-622b populates a sparsely populated region of sub-Jovian planets with measured spin-orbit angles orbiting stars above the Kraft break, while K2-237b’s polar configuration strengthens tentative evidence for preferential orbital orientations. All three systems are compelling targets for future atmospheric characterization, where these dynamical constraints will be vital for a comprehensive understanding of their formation and evolution.

Key words. Techniques: radial velocities – Planets and satellites: gaseous planets – Planets and satellites: atmospheres – Planet-star interactions – Planets and satellites: individual: WASP-35b, TOI-622b, K2-237b

1. Introduction

The upcoming PLANetary Transits and Oscillations of stars (PLATO) mission (Rauer et al. 2025) is expected to discover tens of thousands of exoplanetary candidates. To facilitate their vetting and characterization, dedicated instruments and projects are being developed, such as the Ground-based Observation Programme¹. PLATOSpec² (Kabath et al., in prep.) is a new high-resolution spectrograph that was developed and commissioned in order to facilitate ground-based follow-up of space missions. Besides performing stellar characterization and measuring the planetary masses and eccentricities, PLATOSpec will be able to provide the projected angles between the orbital plane and the

rotation axis of the star (or spin-orbit angles) – a key aspect of the orbital architecture (Albrecht et al. 2022).

To explain the observed population of exoplanets on short orbits, an unknown fraction of gaseous planets is expected to undertake migration after their formation beyond the snow line towards the host star (Ida & Lin 2004; Fabrycky & Tremaine 2007; Baruteau et al. 2014). The two main migration scenarios are disc-free migration (high-eccentricity migration) and disc migration (Baruteau et al. 2014; Dawson & Johnson 2018). However, the occurrence rate of each migration mechanism is still poorly understood. This precludes us from refining our planet formation models in great detail and describing the observed demographics of exoplanets (Madhusudhan et al. 2016; Raymond & Morbidelli 2022).

The spin-orbit angle has emerged in recent years as a powerful probe to study exoplanets and their evolution (Triaud 2018).

¹ <https://warwick.ac.uk/fac/sci/physics/research/astro/plato-science/research/researchareas/followup/>
² <https://stel.asu.cas.cz/plato/spectrograph.html>

Complementarily to other physical and orbital parameters, it provides information about the system’s history. The Solar System has a low spin-orbit angle of around 7 degrees (Beck & Giles 2005). This non-zero value is usually attributed to the non-quiet history of the Solar System (Bailey et al. 2016). The projected spin-orbit angle (λ) is most commonly measured using the Rossiter-McLaughlin (R-M) effect (Rossiter 1924; McLaughlin 1924) with high-resolution spectroscopy. Previous studies have revealed various orientations of the planetary orbits, ranging from perfectly aligned to orbits with polar and retrograde orientation suggesting numerous mechanisms are sculpting these orbits (Crida & Batygin 2014). The availability of precise high-resolution data has led to an increase in the available measurements in recent years (e.g., Bourrier et al. 2023; Zak et al. 2024a). The number of projected spin-orbit angle measurements approaches 300³. Despite this abundance, the understanding of the distribution of these angles remains elusive as several trends were proposed but not confirmed.

The distribution of spin-orbit angles appears to be shaped by distinct physical processes depending on stellar and planetary properties. For hot Jupiters, a clear trend has been observed: those orbiting cool stars tend to have their orbits aligned, while those around hot stars exhibit a broad range of spin-orbit angles (Winn et al. 2010). This pattern is widely thought to be a consequence of tidal realignment, a mechanism that is less effective for planets orbiting hot stars with radiative envelopes (Albrecht et al. 2012). However, our understanding is limited when it comes to sub-Jovian planets, as there is a notable lack of spin-orbit measurements for this population around hot stars, making a direct comparison impossible. Framework proposed by Hixenbaugh et al. (2023) suggests that hotter, more massive stars are more likely to form multiple planets. Subsequent planet-planet scattering and secular interactions within these systems could then excite large spin-orbit misalignment. This hypothesis leads to the prediction that a significant portion of low-mass planets orbiting hot stars should have misaligned orbits.

Albrecht et al. (2021) suggested that certain orbital architectures might be preferred, especially around the polar configuration. Several mechanisms (e.g., Lai 2012; Chen et al. 2024; Louden & Millholland 2024) were suggested to explain this trend, but more measurements are needed to verify such inferences as well as to break degeneracies and deliver a more complete understanding of, e.g., the origin of aligned but eccentric Warm Jupiters (Rice et al. 2022; Espinoza-Retamal et al. 2023; Bieryla et al. 2025). It is highly warranted to obtain measurements of misaligned planets covering the full parameter space to avoid biases (Espinoza-Retamal et al. 2024) and check for differences between various exoplanetary populations to address whether the mechanisms shaping the spin-orbit distribution of Jovian planets are the same as for sub-Jovian planets. For example, Petrovich et al. (2020) suggested disc-driven resonance mechanism exciting the orbit of Neptunian planets with an outer gas giant. Such a mechanism is expected to be inefficient for Jovian planets.

In this work, we present three projected spin-orbit angle measurements of gaseous planets with the newly commissioned PLATOSpec spectrograph. All three are on the Tier 3 (planets selected for detailed studies) target candidate list of the *Ariel* mission and represent good targets for atmospheric characterization.

2. Data sets and their analyses

2.1. Datasets

We have used the PLATOSpec instrument (Kabath et al., in prep.) mounted on the ESO 1.52 m telescope (E152) at the La Silla Observatory, Chile⁴. PLATOSpec is a fiber-fed echelle spectrograph placed in a thermally controlled environment that uses simultaneous ThAr wavelength calibration to provide precise RV measurements. As presented in Kabath et al. (2022), the main role of PLATOSpec will be to provide support to space-based missions such as *PLATO* and *Ariel*. Among the primary science goals will be planetary candidate vetting and detection and subsequent characterization of gas giant planets. This is nicely illustrated in our target selection as one of the systems (TOI-622) is located in the LOPS2⁵ *PLATO* field (Nascimbeni et al. 2025). The wavelength coverage of the instrument spans from 380 to 680 nm, with a resolving power of $R \approx 70\,000$, corresponding to 4.3 km s^{-1} per resolution element. Table 1 shows the properties of the data sets we used. We combined the results from multiple nights when available; no RV offsets between the nights were included in the fit. The PLATOSpec spectra were reduced by the CERES+ pipeline based on the CERES pipeline (Brahm et al. 2017). The spectra are already corrected to the Solar system barycentric frame of reference. The radial velocities were also obtained from the CERES+ pipeline together with their uncertainties and are listed in Appendix B in Tables B.1 to B.3. Table 2 displays the properties of the systems we study.

2.2. Rossiter–McLaughlin effect

The R-M effect causes a spectral line asymmetry, or, equivalently, an asymmetry in the cross-correlation function (CCF) that manifests as anomalous radial velocities during the transit of the exoplanet. To measure the projected spin-orbit angle of the planet (λ), we followed the methodology of Zak et al. (2024b, 2025b): we fitted the RVs with a composite model, which includes a Keplerian orbital component as well as the R-M anomaly. This model is implemented in the ARoMEPy⁶ (Sedaghati et al. 2023) package, which utilizes the RADVEL python module (Fulton et al. 2018) for the formulation of the Keplerian orbit. ARoMEPy is a Python implementation of the R-M anomaly described in the ARoME code (Boué et al. 2013). We used the R-M effect function defined for RVs determined through the cross-correlation technique in our code. We set Gaussian priors for the RV semi-amplitude (K) and the systemic velocity (Γ).

In the R-M effect model, we fixed the following parameters to values reported in the literature: the orbital period (P), the planet-to-star radius ratio (R_p/R_s), and the eccentricity (e). The parameter σ , which is the width of the CCF and represents the effects of the instrumental and turbulent broadening, was measured on the data and fixed. Furthermore, we used the *ExoCTK*⁷ tool to compute the quadratic limb-darkening coefficients with ATLAS9 model atmospheres (Castelli & Kurucz 2003) in the wavelength range of the PLATOSpec instrument (380–680 nm). We set Gaussian priors using the literature value and uncertainty derived from transit modeling (Tab. 2) on the following parameters during the fitting procedure: the central transit time (T_C),

⁴ <https://www.eso.org/public/teles-instr/lasilla/152metre/>

⁵ Long-duration Observation Phase

⁶ <https://github.com/esedagha/ARoMEpy>

⁷ <https://github.com/ExoCTK/exoctk>

³ Retrieved from the TEPcat catalog (Southworth 2011).

Table 1: Observing logs for the three systems. The number in parenthesis represents the number of frames taken in-transit.

Target	Night Obs	No. frames	Exp. Time (s)	Airmass range	Median SNR ^a
WASP-35	2025-01-05/06	17 (10)	1200	1.17-1.09-1.97	28-50
	2025-01-24/25	17 (11)	900-1020	1.09-2.20	22-33
TOI-622	2025-02-09/10	11 (10)	900	1.17-1.84	96-110
	2025-04-27/28	17 (14)	900	1.07-1.86	90-141
K2-237	2025-03-17/18	10 (6)	1200-1750	1.67-1.00	23-52
	2025-04-21/22	12 (6)	1600	1.52-1.00-1.04	28-34
	2025-05-04/05	18 (9)	1200	1.17-1.00-1.37	20-26

Notes. ^(a) Signal-to-noise ratio (SNR) in the extracted spectrum, per spectral resolution element in the order at 515nm.

the orbital inclination (i), and the scaled semi-major axis (a/R_s). Gaussian priors were set on the projected stellar rotational velocity ($v \sin i_*$) and uniform priors on the sky-projected angle between the stellar rotation axis and the normal of the orbital plane (λ).

To obtain the best fitting values of the parameters, we employed three independent Markov chain Monte Carlo (MCMC) ensemble simulations relying on the INFER⁸ implementation that uses the Affine-Invariant Ensemble Sampler. We initialized the MCMC at parameter values found by the Nelder-Mead method perturbed by a small value. We used 20 walkers each with 12 500 steps, burning the first 2 500. As a convergence check, we ensured that the Gelman-Rubin statistics (Gelman & Rubin 1992) is less than 1.001 for each parameter. Using this setup we obtain our results and present them in Sect. 3 and in Figs. 1 to 3.

3. Projected spin-orbit angles of WASP-35b, TOI-622b and K2-237b

We measured the projected spin-orbit angle (λ) of three gaseous planets. WASP-35b was previously studied by Zak et al. (2025a) and we show PLATOSpec data of WASP-35 to display the capabilities of the new instrument. We provide measurements of two targets for the first time: TOI-622b and K2-237b.

WASP-35b is an inflated hot Jupiter orbiting a F9V host star on a short 3.2-day orbit (Enoch et al. 2011). In our analysis, we infer an aligned orbit of WASP-35b with $\lambda = 1^{+19}_{-18}$ deg. This is in good agreement with the one measured by Zak et al. (2025a), who inferred $\lambda = -5 \pm 11$ deg using HARPS-N.

Our result comes from two transits observed with the PLATOSpec instrument while the result from Zak et al. (2025a) uses a single transit with HARPS-N mounted on the 3.58 m Telescope Nazionale Galileo (TNG). The weather was excellent with a sub-arcsec seeing on all three nights. During the first PLATOSpec transit night with 1200s exposures, the RV uncertainties of WASP-35 vary between 11.8 and 20.1 m/s with a median uncertainty of 14.7 m/s. The RV uncertainties from HARPS-N data vary between 3.1 m/s and 9.3 m/s with a median uncertainty of 4.3 m/s and an exposure time of 600s. Factoring in the smaller collecting aperture (factor of 5.6) of the 1.52 m telescope and longer exposure time of the PLATOSpec observations (factor of two), PLATOSpec collected roughly one-third of the photons of HARPS-N. Since the RV error scales as $(S/N)^{-1}$, the expected RV precision of a HARPS-N-like instrument on the 1.52 m telescope should be 5 - 15 m/s. This speaks well for the performance of PLATOSpec.

We show the comparison between the individual PLATOSpec and HARPS-N data in the Appendix in Fig. A1. Finally, we performed a joint fit using both HARPS-N and PLATOSpec data, yielding $\lambda = -4 \pm 10$ deg. We show the posterior of the obtained projected spin-orbit angle and projected rotational velocity for each dataset as well as the joint fit in Fig. A2 of the Appendix.

TOI-622 is a sub-Jovian planet orbiting a F6V host star on a 6.4-day orbit, as reported by Psaridi et al. (2023), who also noticed that despite the high insolation flux (F_\oplus) and adolescent age (< 1 Gyr, Kounkel et al. 2020; Psaridi et al. 2023), TOI-622b does not display an inflated radius, contrarily to what is commonly observed in highly irradiated planets. However, the inflated radius' origin and the dependency on the orbital parameters is still not fully understood (Thorngren 2024). In our analysis, we infer an aligned orbit for TOI-622b with $\lambda = -4 \pm 12$ deg.

K2-237b is a hot Jupiter orbiting a F6V host star on a 2.1-day orbit (Soto et al. 2018; Smith et al. 2019). Shan et al. (2023) identified significant transit timing variations (TTV) by combining K2 and TESS data. The TTVs were also detected by Yang et al. (2024) who also derived orbital period decay. We infer a polar orbit with spin-orbit angle $\lambda = 91 \pm 7$ deg.

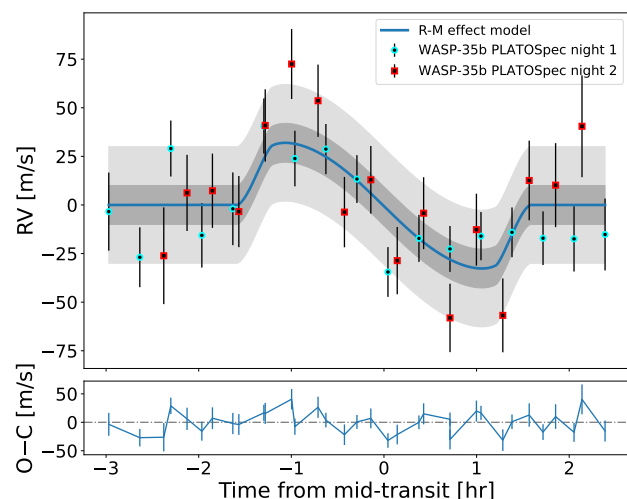


Fig. 1: R-M effect of WASP-35b observed with PLATOSpec. The observed data points – colored according to the respective night they were obtained – are shown with their error bars. The systemic and Keplerian orbit velocities were removed. The blue line shows the best fitting model to the data, together with 1- σ (dark grey) and 3- σ (light grey) confidence intervals.

⁸ <https://github.com/nealegibson/Infer>

Table 2: Properties of the targets (star and planet).

	Parameters	WASP-35	TOI-622	K2-237
Star	V mag	10.95 ± 0.09	8.995 ± 0.002	11.60 ± 0.05
	Sp. Type	F9V	F6V	F6V
	M_s (M_\odot)	1.106 ± 0.015	1.313 ± 0.079	1.256 ^{+0.055} _{-0.062}
	R_s (R_\odot)	1.122 ± 0.016	1.415 ± 0.047	1.236 ^{+0.043} _{-0.036}
	T_{eff} (K)	6072 ± 63	6400 ± 100	6180 ⁺¹⁶⁰ ₋₁₄₀
	$v \sin i_*$ (km/s)	2.4 ± 0.6	19.0 ± 0.9	11.76 ± 0.90
	Planet	M_p (M_{Jup})	0.765 ± 0.029	0.303 ^{+0.069} _{-0.072}
R_p (R_{Jup})		1.349 ± 0.022	0.824 ^{+0.028} _{-0.029}	1.433 ^{+0.056} _{-0.049}
Period (d)		3.1615691 ± 0.0000003	6.402513 ^{+0.000031} _{-0.000054}	2.18053332 ^{+0.00000054} _{-0.00000054}
$T_0 - 2450000$ (d)		5531.47920 ± 0.00029	8520.69176 ^{+0.00031} _{-0.00046}	7706.61618 ^{+0.00003} _{-0.00003}
a (AU)		0.04360 ± 0.00020	0.078 ^{+0.0052} _{-0.0059}	0.03552 ^{+0.00051} _{-0.00060}
e		0	0	0
i (deg)		87.95 ^{+0.33} _{-0.33}	86.62 ^{+0.77} _{-0.54}	88.37 ^{+1.0} _{-0.88}
T_{eq} (K)		1484 ± 18	1388 ⁺²² ₋₂₂	1759 ⁺⁴⁹ ₋₄₂
Discovery ref.		Enoch et al. (2011)	Psaridi et al. (2023)	Soto et al. (2018)
Prior ref.		Bai et al. (2022)	Psaridi et al. (2023)	Thygesen et al. (2023)

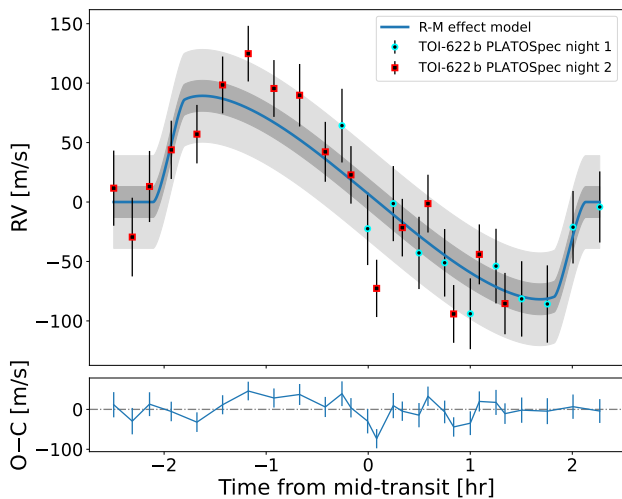


Fig. 2: Same as Fig. 1 for TOI-622.

The results of our fits are shown in Figs. 1 to 3, while the MCMC results are shown in the Appendix in Figs. A3 to A5. The derived values from the MCMC analysis are displayed in Table 3.

4. Discussion

4.1. Stellar rotation and true spin-orbit angle ψ

The projected spin-orbit angle derived through the R-M effect characterizes the architecture with a more accurate description than mutual inclinations of planes in multiplanetary systems. However, what is desirable is the true (3D) spin-orbit angle, ψ , and not just the projected angle. This requires a knowledge of the stellar inclination angle.

The stellar inclination can be derived from the stellar rotation period, radius, and projected rotational velocity. One of the best ways to determine the rotation period is by using photometry to study the rotational modulation of the host stars due to, e.g., stellar spots (Skarka et al. 2022). Once the stellar inclination is known, the true spin-orbit angle, ψ (i.e., the

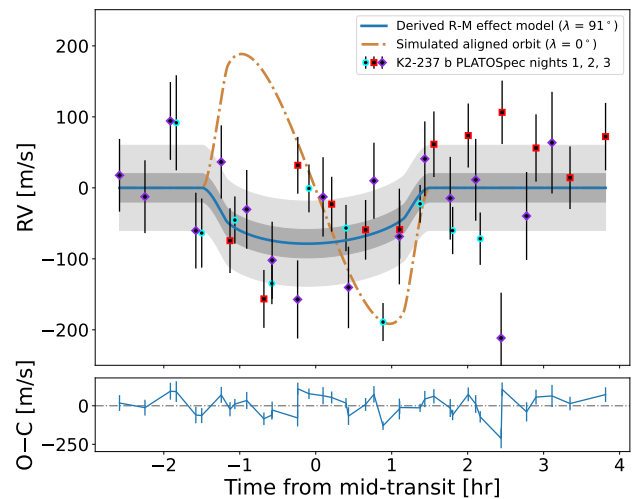


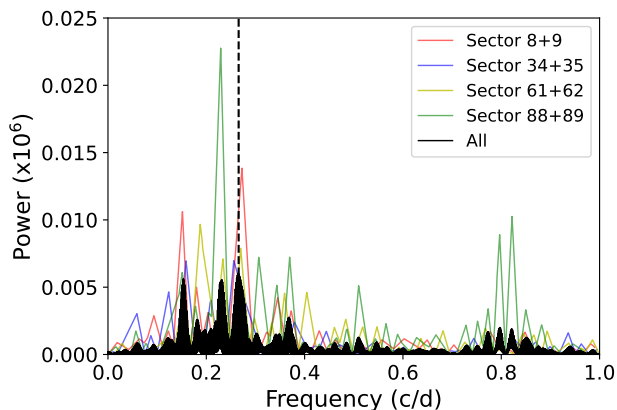
Fig. 3: Same as Fig. 1 for K2-237b. Additionally, we show an aligned orbit (brown color) for illustration that is clearly disfavored by the data.

angle between the stellar spin-axis and the normal to the orbital plane) can be inferred using the spherical law of cosines, $\cos \psi = \sin i_* \sin i \cos |\lambda| + \cos i_* \cos i$, with the approach suggested by Masuda & Winn (2020) to account for the dependency between v and $v \sin i_*$. A rotational period of 5.07 ± 0.02 d was previously determined for K2-237 from K2 mission data (Soto et al. 2018). We attempted to derive the stellar rotation period and additional variability for WASP-35 and TOI-622 by performing Lomb-Scargle periodograms on the *TESS* (Ricker et al. 2015) data and ASAS-SN *g*-band light curves (Kochanek et al. 2017) using PERIOD04 (Lenz & Breger 2004).

We do not find any significant periodic signals for WASP-35. For TOI-622, we investigated data from the *TESS* Science Processing Operations Center (SPOC) and Quick Look pipeline (QLP) pipelines (Jenkins et al. 2016; Huang et al. 2020a,b). The data were available in 8 sectors (8+9, 34+35, 61+62 and 88+89) in both long and short cadences (data with a cadence of 1800, 600, 200 and 120 seconds). We investigated all available data sets and excluded the QLP data due to strong artifacts and trends.

Table 3: MCMC analysis results for selected exoplanets. \mathcal{N} denotes priors with a normal distribution and \mathcal{U} priors with a uniform distribution.

Parameter	Prior	WASP-35b	Prior	TOI-622b	Prior	K2-237b
$T_c - 2450000$ [d]	$\mathcal{N}(T_0, 0.006)$	10681.6770 ± 0.0005	$\mathcal{N}(T_0, 0.006)$	10729.5639 ± 0.0038	$\mathcal{N}(T_0, 0.006)$	$10752.8178^{+0.0073}_{-0.0083}$
λ [deg]	$\mathcal{U}(-180, 180)$	1^{+18}_{-19}	$\mathcal{U}(-180, 180)$	-4^{+12}_{-12}	$\mathcal{U}(-180, 180)$	91 ± 7
$v \sin i_*$ [km/s]	$\mathcal{N}(2.4, 0.6)$	$2.40^{+0.36}_{-0.35}$	$\mathcal{N}(19.0, 0.9)$	$19.4^{+0.83}_{-0.86}$	$\mathcal{N}(11.76, 0.90)$	$11.67^{+0.90}_{-0.90}$
a/R_s	$\mathcal{N}(8.36, 0.13)$	8.32 ± 0.12	$\mathcal{N}(10.64, 0.85)$	$10.97^{+0.56}_{-0.58}$	$\mathcal{N}(6.18, 0.19)$	$6.16^{+0.19}_{-0.19}$
i [deg]	$\mathcal{N}(87.95, 0.33)$	88.09 ± 0.32	$\mathcal{N}(86.62, 0.77)$	$87.55^{+0.51}_{-0.52}$	$\mathcal{N}(88.37, 1.0)$	$88.11^{+0.59}_{-0.60}$
Γ [km/s]	$\mathcal{N}(17.73, 0.20)$	17.754 ± 0.005	$\mathcal{N}(15.80, 0.20)$	$15.900^{+0.011}_{-0.012}$	$\mathcal{N}(-22.45, 0.20)$	$-22.347^{+0.017}_{-0.016}$
K [km/s]	$\mathcal{N}(0.09, 0.05)$	0.078 ± 0.030	$\mathcal{N}(0.03, 0.05)$	$0.049^{+0.047}_{-0.048}$	$\mathcal{N}(0.18, 0.10)$	$0.113^{+0.065}_{-0.062}$


 Fig. 4: TOI-622 frequency spectra of the SPOC *TESS* full data set (black) and from different sectors (colors). The vertical line shows the position of the rotation frequency.

After removing the transits, we performed a frequency analysis to search for significant periodic variability. According to [Pсариди et al. \(2023\)](#), the rotational period of TOI-622 estimated from $v \sin i_*$ should be 3.77 days (0.265 c/d). This frequency is the strongest one in the *TESS* SPOC 2-minute cadence data and has a $SNR = 5.1^9$, that is above the significance level of $SNR = 4$ ([Breger et al. 1993](#)). In addition, this peak is apparent in the SPOC long-cadence data and is present in frequency spectra of all sectors when analyzed separately (see Fig. 4), although at slightly different positions. This can be a sign of differential rotation. To conclude, we consider the peak at 0.2658 c/d as the consequence of the rotation of the star.

Subsequently, using the $v \sin i_*$ from the R-M effect analysis we calculate $\psi = 16.1^{+8.0}_{-9.7}$ deg for TOI-622b that further supports the aligned configuration. Furthermore, we calculate $\psi = 90.5^{+6.8}_{-6.2}$ deg for K2-237b. The true spin-orbit measurement confirms the polar orbit for K2-237. In the following sections, we discuss the tidal realignment timescales and possible evolutionary pathways of the studied planets.

4.2. Dynamical timescale

To better understand the evolution of these transiting exoplanets we must compare their age to the tidal circularization and tidal realignment timescales. These can be used to study whether the eccentricity and spin-orbit angle have changed since the formation of the system. It provides only a limit as the processes al-

⁹ False alarm probability, $FAP = 8.2 \times 10^{-8}$ using equation 7.27 from [Hatzes \(2019\)](#), based on an empirical relation of obtaining FAP from the SNR ([Kuschnig et al. 1997](#)).

tering these parameters may not happen at the same time as the system's formation.

WASP-35b is most likely the oldest system in our sample as [Enoch et al. \(2011\)](#) derived an age of 6^{+5}_{-4} Gyr or it. [Pсариди et al. \(2023\)](#) estimated the age of TOI-622 to be 0.9 ± 0.2 Gyr, while [Thygesen et al. \(2023\)](#) inferred an age of $1.09^{+1.50}_{-0.78}$ Gyr for K2-237.

We have used Equation 3 from [Adams & Laughlin \(2006\)](#) to calculate the tidal circularization time scale, τ_{cir} . Assuming a tidal quality factor $Q_p = 10^6$, we derive τ_{cir} equal to ≈ 0.1 Gyr for WASP-35b, ≈ 10 Gyr for TOI-622b and ≈ 0.02 Gyr for K2-237. We thus conclude that only TOI-622b would likely be able to keep any initial eccentricity, while the other two planets have had their orbits circularized.

Next, we compute the tidal realignment timescales. For cool stars with convective envelopes below the Kraft break (an abrupt decrease in the stars' average rotation rates at about 6200 K, [Kraft 1967](#)), the tidal alignment timescale can be approximated ([Albrecht et al. 2012](#)) as:

$$\tau_{\text{CE}} = \frac{10^{10} \text{ yr}}{\left(\frac{M_p}{M_*}\right)^2} \left(\frac{a/R_*}{40}\right)^6. \quad (1)$$

This allows us to compute the tidal realignment timescale for WASP-35b as $\tau_{\text{CE}} \approx 10^{12}$ yr.

Stars above the Kraft break have radiative envelopes with less efficient tidal forces. Hence, a different formula should be used to calculate the tidal realignment timescales. TOI-622 has an effective temperature of 6400 K and is clearly located above the Kraft break. The effective temperature of K2-237 (6257 ± 100 K ([Soto et al. 2018](#)) and 6180^{+160}_{-140} ([Thygesen et al. 2023](#))) is just around the division. However, as presented in [Spalding & Winn \(2022\)](#) the division between radiative and convective envelopes is also metallicity dependent (their Fig. 9), and so the derived super-solar metallicity of K2-237 places the K2-237 above the Kraft break.

For these two systems, we used the following formula ([Albrecht et al. 2012](#)) to calculate τ_{RA} :

$$\tau_{\text{RA}} = \frac{5}{4} \cdot 10^9 \text{ yr} \left(\frac{M_p}{M_*}\right)^{-2} \left(1 + \frac{M_p}{M_*}\right)^{-5/6} \left(\frac{a/R_*}{6}\right)^{17/2}, \quad (2)$$

leading to $\tau_{\text{RA}} \approx 10^{18}$ yr for TOI-622b and $\approx 10^{15}$ yr for K2-237b.

The much longer tidal realignment timescales compared to the age of the studied systems suggest that the spin-orbit angle has not changed since its initial value. This is especially interesting for K2-237b, as it suggests that the planet's polar orbit was established by some initial dynamical events rather than being a later result of tidal realignment.

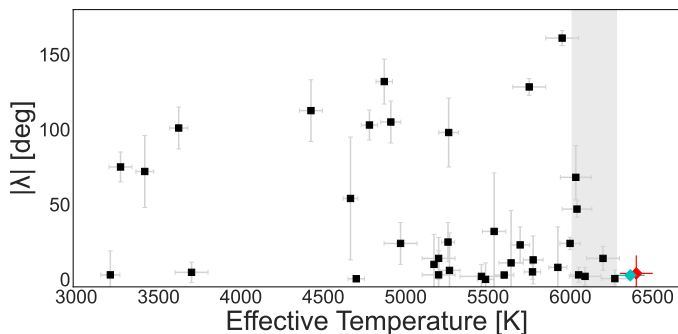


Fig. 5: Projected spin-orbit angle versus stellar effective temperature for the sub-Jovian population ($M_p \lesssim 0.3 M_{\text{Jup}}$). The gray area shows the position of the Kraft break as derived in Spalding & Winn (2022). The literature values were retrieved from the TEPcat catalogue (Southworth 2011). TOI-622b is plotted in red. TOI-622b joins the rare population of sub-Jovian planets around hot stars, and similarly to HD 106315c (cyan), orbits a star located above the Kraft break.

4.3. Evolutionary scenarios and spin-orbit distribution

WASP-35b was studied by Zak et al. (2025a) with the HARPS-N instrument. They derived an aligned orbit consistent with quiet disc migration. Our result using a smaller, 1.52 m telescope is in good agreement with the previous result (Figs. A1 and A2).

TOI-622b The low spin-orbit angle of TOI-622b together with zero eccentricity and the long circularization and realignment timescales are indicative of the quiet evolution of the system in the disc, ruling out mechanisms exciting the planetary eccentricity or the spin-orbit angle.

There is a lack of measurements for Neptunian planets above the Kraft break. TOI-622 belongs to a rare type of system with an F-type star harboring a sub-Jovian planet. The only other example of a Neptunian planet around an F-type star that confidently lies above the Kraft break with spin-orbit angle constrained is HD 106315c (Zhou et al. 2018; Bourrier et al. 2023). Spin-orbit angle measurement of a sub-Saturn around a more massive star exists, such as TOI-1842b with $M_s = 1.45^{+0.07}_{-0.14} M_{\odot}$, for which Hixenbaugh et al. (2023) measured $\lambda = -68.1^{+21.2}_{-14.7}$ deg and $\psi = 73.3^{+16.3}_{-12.9}$ deg. However, the host star is an evolved subgiant with $T_{\text{eff}} = 6033^{+95}_{-93}$ K, an evolutionary stage for which the Kraft break is no longer applicable. They proposed a hypothesis that hot/massive stars ($M_s > 1.2 M_{\odot}$) would have a prevalence of misaligned systems. Our result does not fit in this trend.

As can be seen from Fig. 5, more sub-Jovian planets orbiting a star above the Kraft break are needed to explore the shaping mechanisms in this parameter space as it is less affected by tidal realignment. However, finding smaller planets around hotter stars is a challenging prospect. We queried the NASA database to check how many such systems would be available for spin-orbit follow-up. We imposed conditions of a transiting planet around a star brighter than 12 V_{mag} around a star hotter than 6180 K (above the Kraft break) with the following properties: $R_p \gtrsim 2 R_{\oplus}$, $M_p \lesssim 0.3 M_{\text{Jup}}$. This resulted in 10 systems meeting the conditions that are currently available for a follow-up to determine their spin-orbit angle. A dedicated program could easily achieve measuring the projected spin-orbit angle for most of them with current 4-m and 8-m class telescopes. Deriving their true-spin orbit angles via determination of the stellar inclination might however be challenging as F-type stars display complex

behavior where rotation is mixed with various types of pulsations (e.g., Henriksen et al. 2023). Long-term photometric monitoring to fully explain the power spectrum in Fig. 4 is highly warranted. In this respect, the *PLATO* mission will substantially help, in particular for TOI-622 as it is located in the LOPS2 field (Nascimbeni et al. 2025) that will be observed for at least two continuous years.

K2-237b is a typical hot Jupiter. Its host star lies on the boundary between having a convective and a radiative envelope; the former would result in significantly more efficient tidal forces. However, the derived timescales suggest that the spin-orbit angle should not be affected regardless of the inner stellar structure. Yang et al. (2024) using the detected TTVs and period decay rate suggested that K2-237b has undergone disc migration. We find transit timing consistent with their results, although our uncertainty on the timing does not allow us to further refine the ephemeris. However, in this work we derive a polar orbit that is rather indicative of disc-free migration (Fabrycky & Tremaine 2007) as disc migration is less likely to produce such a highly misaligned orbit. We have checked Gaia DR3 (Gaia Collaboration et al. 2023) data in search of a companion that could perturb planet’s orbit but none of the stars in the proximity are consistent with a physically bound companion. Furthermore, the Renormalised Unit Weight Error (RUWE)¹⁰ value ≈ 0.98 does not suggest binarity. Without the presence of a bound companion, we cannot unequivocally rule out disc migration.

The K2-237 system adds another piece of evidence for the “Preponderance of Perpendicular Planets” (Albrecht et al. 2021) suggesting some orbital configurations are preferred. This trend – if indeed real (Dong & Foreman-Mackey 2023; Siegel et al. 2023) – is still not understood and neither are the mechanisms shaping it (Attia et al. 2023; Knudstrup et al. 2024). Such a prevalence has been suggested both for Jupiters and Neptunians, yet the mechanisms responsible for their origin seem to be different. As detailed in Petrovich et al. (2020), the disc-driven resonances proposed to alter the spin-orbit angle of Neptunian planets would be inefficient for more massive planets.

Despite its polar orbit, disc-free migration for K2-237b is not unambiguously confirmed. An alternative explanation may lie in the system’s early evolution. The traditional picture assumes a single star and its disc inherit their spin orientation from the initial collapse of a prestellar core and that this alignment is preserved. However, this idealized view often overlooks that the system’s initial conditions can be altered by subsequent evolution and interactions with the surrounding environment. Early planet formation is not fully understood, and processes that warp or tilt the disc—potentially caused by stellar magnetic fields, fly-by encounters, or other phenomena—might shape exoplanet populations in ways not yet fully explored (Foucart & Lai 2011; Romanova et al. 2013; Batygin 2012; Matsakos & Königl 2017). One such environmental mechanism capable of breaking the initial stellar-disc alignment is the late infall of material onto the system (Bate et al. 2010; Thies et al. 2011; Fielding et al. 2015; Kuffmeier et al. 2021).

Kuffmeier et al. (2024) have shown that the infall might be capable of creating polar orbits such as the one of K2-237b. Additionally, they have found that the misalignment due to infall

¹⁰ This parameter captures the astrometric deviations from single-source solutions. See https://gea.esac.esa.int/archive/documentation/GEDR3/Gaia_archive/chap_datamodel/sec_dm_main_tables/ssec_dm_gaia_source.html#gaia_source-ruwe for a detailed definition. A value close to 1 indicates that the astrometric solution is valid.

correlates with stellar mass. Higher mass stars take longer to settle into their final spin orientation compared to lower mass stars. During this settling, the late infall can occur, more easily producing misaligned planets. The combined effect of tidal realignment, which is more efficient for stars below the Kraft break (with convective envelopes), and late infall will produce a distribution of exoplanets with misaligned planets preferentially around stars above the Kraft break ($\gtrsim 1.2 M_{\odot}$), although on vastly different timescales. A promising way to distinguish the dominant mechanism would be to explore the spin-orbit of young planets where the tidal realignment did not have sufficient time to act upon, while the late-infall would have already concluded, alongside the disappearance of the protoplanetary disc. The recent discovery of a 3 Myr old transiting exoplanet with a misaligned disc and the presence of a stellar companion (Barber et al. 2024) support the complex interplay of several mechanisms forming the spin-orbit distribution (Nealon et al. 2025).

The true origin of the evolution of K2-237b will be unlocked by obtaining additional data: i) searching for the additional companion responsible for the TTVs or one that would be able to produce misaligned orbit by gravitational interaction (Kozai-Lidov mechanism) ii) allowing for detailed atmospheric composition constraining the accretion mechanisms onto the planet during the disc stage. The elemental abundance ratios such as C/O, N/O, S/N (Öberg et al. 2011; Turrini et al. 2021; Pacetti et al. 2022) are indicative of previous migration mechanisms. For example, the detection of a high C/O ratio with the JWST or the upcoming *Ariel* mission would serve as additional evidence of the disc-free migration scenario. While a low C/O ratio would rather be indicative of disc migration where the planet accretes oxygen-rich solids that alter the initial composition.

Finally, obtaining the spin-orbit angle measurements is highly complementary to atmospheric studies using space missions such as *JWST* and *Ariel* as planetary migration is expected to alter both the spin-orbit angle and chemical composition (Madhusudhan et al. 2014). However, their exact interplay is not fully understood and should be performed at the population level (Kirk et al. 2024). Zak et al. (2025a) identified a lack of spin-orbit angle measurements within the *Ariel* Mission candidate sample (MCS) list, as over 70% of candidates do not have their spin-orbit measured. Within Tier 3 candidates (those that will be selected for detailed atmospheric studies over multiple visits) this was only 30%.

All three targets in this work are listed on the *Ariel* MCS list among Tier 3 candidates (Edwards & Tinetti 2022) and our results can serve as an additional parameter for the final target selection as well as for the subsequent interpretation of the measured atmospheric composition showcasing the synergy between ground- and space-based observations.

5. Summary

The migration pathways of gaseous planets, together with the mechanisms shaping the spin-orbit angle distribution, are still unconstrained. We present measurements of the projected spin-orbit angle of three gaseous exoplanets. We have used the newly commissioned PLATOSpec instrument mounted at the E152 Telescope at La Silla Observatory. We measure the projected spin-orbit angle for WASP-35b to demonstrate the capability of PLATOSpec and find excellent agreement with HARPS-N literature data. Furthermore, we measure the projected spin-orbit angle of TOI-622b and K2-237b for the first time. We derive an aligned orbit for TOI-622b and a nearly perfect polar orbit for K2-237b. We also derive the true spin-orbit angle ψ for TOI-622

and K2-237b. We infer that the previous evolution of TOI-622b is consistent with quiet disc migration. In contrast to previous work, we suggest that K2-237b has likely undergone disc-free migration. Both systems are valuable pieces in the spin-orbit distribution and the quest for its understanding. TOI-622b is located in the sparsely populated region of sub-Jovian planets with spin-orbit angle measurement orbiting stars above the Kraft break. More data are needed to characterize the spin-orbit distribution of sub-Jovian planets around hot stars and how it differs from the one of Jovian planets. K2-237b's polar orbit strengthens the tentative existence of preferential orientations of planetary orbits. Furthermore, all three targets are prime targets for future atmospheric characterization. Finally, our results highlight the capability of the PLATOSpec as a successful instrument that is able to provide ground-based support to *PLATO*, *Ariel*, and other space missions in years to come.

Acknowledgements. The authors thank the anonymous referee for helpful comments that improved the quality of the manuscript. JZ and PK acknowledge support from GACR:22-30516K. The research of PG was supported by the Slovak Research and Development Agency under contract No. APVV-20-0148 and the internal grant No. VVGS-2023-2784 of the P. J. Šafárik University in Košice funded by the EU NextGenerationEU through the Recovery and Resilience Plan for Slovakia under the project No. 09I03-03-V05-00008. LV acknowledges the support from ANID Fondecyt n. 1211162, Fondecyt n. 1251299, and BASAL FB210003. AB is supported by the Italian Space Agency (ASI) with *Ariel* grant n. 2021.5.HH.0. RB acknowledges support from FONDECYT Project 1241963 and from ANID – Millennium Science Initiative – ICN12_009. DI acknowledges support from collaborations and/or information exchange within NASA's Nexus for Exoplanet System Science (NEXSS) research coordination network sponsored by NASA's Science Mission Directorate under agreement no. 80NSSC21K0593 for the programme 'Alien Earths'. PLATOSpec was built and is operated by a consortium consisting of the Astronomical Institute ASCR in Ondřejov, Czech Republic (ASU), the Thüringer Landessternwarte (Thuringian State Observatory - Germany), the Universidad Católica in Chile (PUC - Chile), and minor partners include Masaryk University (Czechia), Universidad Adolfo Ibáñez (Chile) and Institute for Plasma Physics of the Czech Academy of Sciences (Czechia). Financing for the modernisation and front end of the 1.52-m telescope was provided by ASU and personal costs were partly financed from grant LTT-20015. Financing for the construction of PLATOSpec was provided by the Free State of Thuringia, under the "Directive for the Promotion of Research PUC is acknowledging the support from ANID Fondecyt n. 1211162 and n. 1251299, and ANID QUIMAL ASTRO20-0025. Use of the 1.52-m telescope was made possible through an agreement between ESO and the PLATOSpec consortium.

References

- Adams, F. C. & Laughlin, G. 2006, *ApJ*, 649, 1004
 Albrecht, S., Winn, J. N., Johnson, J. A., & et al. 2012, *ApJ*, 757, 18
 Albrecht, S. H., Dawson, R. I., & Winn, J. N. 2022, *PASP*, 134, 082001
 Albrecht, S. H., Marcussen, M. L., Winn, J. N., & et al. 2021, *ApJ*, 916, L1
 Attia, O., Bourrier, V., Delisle, J. B., & et al. 2023, *A&A*, 674, A120
 Bai, L., Gu, S., Wang, X., et al. 2022, *AJ*, 163, 208
 Bailey, E., Batygin, K., & Brown, M. E. 2016, *AJ*, 152, 126
 Barber, M. G., Mann, A. W., Vanderburg, A., & et al. 2024, *Nature*, 635, 574
 Baruteau, C., Crida, A., Paardekooper, S. J., et al. 2014, in *Protostars and Planets VI*, ed. H. Beuther, R. S. Klessen, C. P. Dullemond, & T. Henning, 667–689
 Bate, M. R., Lodato, G., & Pringle, J. E. 2010, *MNRAS*, 401, 1505
 Batygin, K. 2012, *Nature*, 491, 418
 Beck, J. G. & Giles, P. 2005, *ApJ*, 621, L153
 Bieryla, A., Dong, J., Zhou, G., et al. 2025, *AJ*, 169, 273

- Boué, G., Montalto, M., Boisse, I., & et al. 2013, *A&A*, 550, A53
- Bourrier, V., Attia, O., Mallonn, M., & et al. 2023, *A&A*, 669, A63
- Brahm, R., Jordán, A., & Espinoza, N. 2017, *PASP*, 129, 034002
- Breger, M., Stich, J., Garrido, R., et al. 1993, *A&A*, 271, 482
- Castelli, F. & Kurucz, R. L. 2003, in *Modelling of Stellar Atmospheres*, ed. N. Piskunov, W. W. Weiss, & D. F. Gray, Vol. 210, A20
- Chen, C., Baronett, S. A., Nixon, C. J., & Martin, R. G. 2024, *MNRAS*, 533, L37
- Crida, A. & Batygin, K. 2014, *A&A*, 567, A42
- Dawson, R. I. & Johnson, J. A. 2018, *ARA&A*, 56, 175
- Dong, J. & Foreman-Mackey, D. 2023, *AJ*, 166, 112
- Edwards, B. & Tinetti, G. 2022, *AJ*, 164, 15
- Enoch, B., Anderson, D. R., Barros, S. C. C., & et al. 2011, *AJ*, 142, 86
- Espinoza-Retamal, J. I., Brahm, R., Petrovich, C., et al. 2023, *ApJ*, 958, L20
- Espinoza-Retamal, J. I., Stefánsson, G., Petrovich, C., et al. 2024, *AJ*, 168, 185
- Fabrycky, D. & Tremaine, S. 2007, *ApJ*, 669, 1298
- Fielding, D. B., McKee, C. F., Socrates, A., Cunningham, A. J., & Klein, R. I. 2015, *MNRAS*, 450, 3306
- Foucart, F. & Lai, D. 2011, *MNRAS*, 412, 2799
- Fulton, B. J., Petigura, E. A., Blunt, S., & et al. 2018, *PASP*, 130, 044504
- Gaia Collaboration, Vallenari, A., Brown, A. G. A., & et al. 2023, *A&A*, 674, A1
- Gelman, A. & Rubin, D. B. 1992, *Statistical Science*, 7, 457
- Hatzes, A. P. 2019, *The Doppler Method for the Detection of Exoplanets*
- Henriksen, A. I., Antoci, V., Saio, H., & et al. 2023, *MNRAS*, 524, 4196
- Hixenbaugh, K., Wang, X.-Y., Rice, M., & Wang, S. 2023, *ApJ*, 949, L35
- Huang, C. X., Vanderburg, A., Pál, A., et al. 2020a, *Research Notes of the American Astronomical Society*, 4, 204
- Huang, C. X., Vanderburg, A., Pál, A., et al. 2020b, *Research Notes of the American Astronomical Society*, 4, 206
- Ida, S. & Lin, D. N. C. 2004, *ApJ*, 604, 388
- Jenkins, J. M., Twicken, J. D., McCauliff, S., et al. 2016, in *Society of Photo-Optical Instrumentation Engineers (SPIE) Conference Series*, Vol. 9913, *Software and Cyberinfrastructure for Astronomy IV*, ed. G. Chiozzi & J. C. Guzman, 99133E
- Kabath, P., Vanzi, L., Hatzes, A., et al. 2022, in *Bulletin of the American Astronomical Society*, Vol. 54, 102.118
- Kirk, J., Ahrer, E.-M., Penzlin, A. B. T., & et al. 2024, *RAS Techniques and Instruments*, 3, 691
- Knudstrup, E., Albrecht, S. H., Winn, J. N., et al. 2024, *A&A*, 690, A379
- Kochanek, C. S., Shappee, B. J., Stanek, K. Z., et al. 2017, *PASP*, 129, 104502
- Koukkel, M., Covey, K., & Stassun, K. G. 2020, *AJ*, 160, 279
- Kraft, R. P. 1967, *ApJ*, 150, 551
- Kuffmeier, M., Dullemond, C. P., Reissl, S., & Goicovic, F. G. 2021, *A&A*, 656, A161
- Kuffmeier, M., Pineda, J. E., Segura-Cox, D., & Haugbølle, T. 2024, *A&A*, 690, A297
- Kuschnig, R., Weiss, W. W., Gruber, R., Bely, P. Y., & Jenkner, H. 1997, *A&A*, 328, 544
- Lai, D. 2012, *MNRAS*, 423, 486
- Lenz, P. & Breger, M. 2004, in *IAU Symposium*, Vol. 224, *The A-Star Puzzle*, ed. J. Zverko, J. Ziznovsky, S. J. Adelman, & W. W. Weiss, 786–790
- Louden, E. M. & Millholland, S. C. 2024, *ApJ*, 974, 304
- Madhusudhan, N., Agúndez, M., Moses, J. I., & Hu, Y. 2016, *Space Sci. Rev.*, 205, 285
- Madhusudhan, N., Amin, M. A., & Kennedy, G. M. 2014, *ApJ*, 794, L12
- Masuda, K. & Winn, J. N. 2020, *AJ*, 159, 81
- Matsakos, T. & Königl, A. 2017, *AJ*, 153, 60
- McLaughlin, D. B. 1924, *ApJ*, 60, 22
- Nascimbeni, V., Piotto, G., Cabrera, J., et al. 2025, *A&A*, 694, A313
- Nealon, R., Smallwood, J. L., Aly, H., et al. 2025, *MNRAS*, 540, L84
- Öberg, K. I., Murray-Clay, R., & Bergin, E. A. 2011, *ApJ*, 743, L16
- Pacetti, E., Turrini, D., Schisano, E., & et al. 2022, *ApJ*, 937, 36
- Petrovich, C., Muñoz, D. J., Kratter, K. M., & et al. 2020, *ApJ*, 902, L5
- Psaridi, A., Bouchy, F., Lendl, M., et al. 2023, *A&A*, 675, A39
- Rauer, H., Aerts, C., Cabrera, J., et al. 2025, *Experimental Astronomy*, 59, 26
- Raymond, S. N. & Morbidelli, A. 2022, in *Astrophysics and Space Science Library*, Vol. 466, *Demographics of Exoplanetary Systems*, *Lecture Notes of the 3rd Advanced School on Exoplanetary Science*, ed. K. Biazzo, V. Bozza, L. Mancini, & A. Sozzetti, 3–82
- Rice, M., Wang, S., Wang, X.-Y., et al. 2022, *AJ*, 164, 104
- Ricker, G. R., Winn, J. N., Vanderspek, R., & et al. 2015, *Journal of Astronomical Telescopes, Instruments, and Systems*, 1, 014003
- Romanova, M. M., Ustyugova, G. V., Koldoba, A. V., & Lovelace, R. V. E. 2013, *MNRAS*, 430, 699
- Rossiter, R. A. 1924, *ApJ*, 60, 15
- Sedaghati, E., Jordán, A., Brahm, R., & et al. 2023, *AJ*, 166, 130
- Shan, S.-S., Yang, F., Lu, Y.-J., et al. 2023, *ApJS*, 264, 37
- Siegel, J. C., Winn, J. N., & Albrecht, S. H. 2023, *ApJ*, 950, L2
- Skarka, M., Žák, J., Fedurco, M., et al. 2022, *A&A*, 666, A142
- Smith, A. M. S., Csizmadia, S., Gandolfi, D., et al. 2019, *Acta Astron.*, 69, 135
- Soto, M. G., Díaz, M. R., Jenkins, J. S., et al. 2018, *MNRAS*, 478, 5356
- Southworth, J. 2011, *MNRAS*, 417, 2166
- Spalding, C. & Winn, J. N. 2022, *ApJ*, 927, 22
- Thies, I., Kroupa, P., Goodwin, S. P., Stamatellos, D., & Whitworth, A. P. 2011, *MNRAS*, 417, 1817
- Thorngren, D. P. 2024, *arXiv e-prints*, arXiv:2405.05307
- Thygesen, E., Ranshaw, J. A., Rodriguez, J. E., et al. 2023, *AJ*, 165, 155
- Triaud, A. H. M. J. 2018, in *Handbook of Exoplanets*, ed. H. J. Deeg & J. A. Belmonte, 2
- Turrini, D., Schisano, E., Fonte, S., & et al. 2021, *ApJ*, 909, 40
- Winn, J. N., Fabrycky, D., Albrecht, S., & Johnson, J. A. 2010, *ApJ*, 718, L145
- Yang, F., Long, R. J., Kerins, E., et al. 2024, *MNRAS*, 535, L7
- Zak, J., Bocchieri, A., Sedaghati, E., & et al. 2024a, *A&A*, 686, A147
- Zak, J., Boffin, H. M. J., Bocchieri, A., et al. 2025a, *arXiv e-prints*, arXiv:2505.20516
- Zak, J., Boffin, H. M. J., Sedaghati, E., et al. 2025b, *A&A*, 694, A91
- Zak, J., Boffin, H. M. J., Sedaghati, E., & et al. 2024b, *A&A*, 687, L2
- Zhou, G., Rodriguez, J. E., Vanderburg, A., et al. 2018, *AJ*, 156, 93

Appendix A: Additional tables and figures

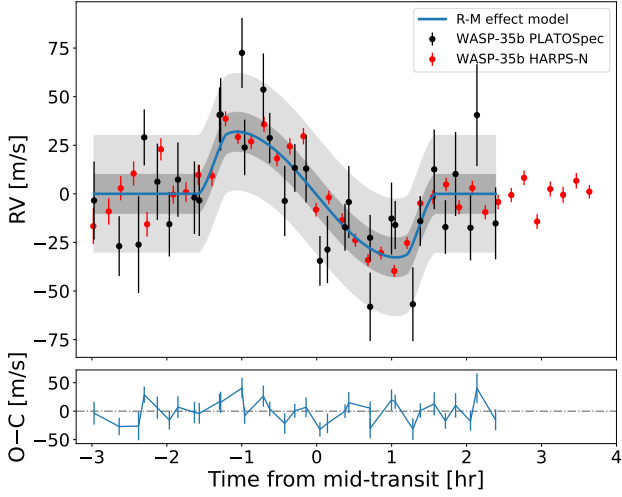


Fig. A1: Same as Fig. 1 but with overlapping 3.6 m/HARPS-N data (Zak et al. 2025a). This illustrates the performance of PLATOSpec and the ability to obtain comparable results on 1.5m telescope with scheduling flexibility.

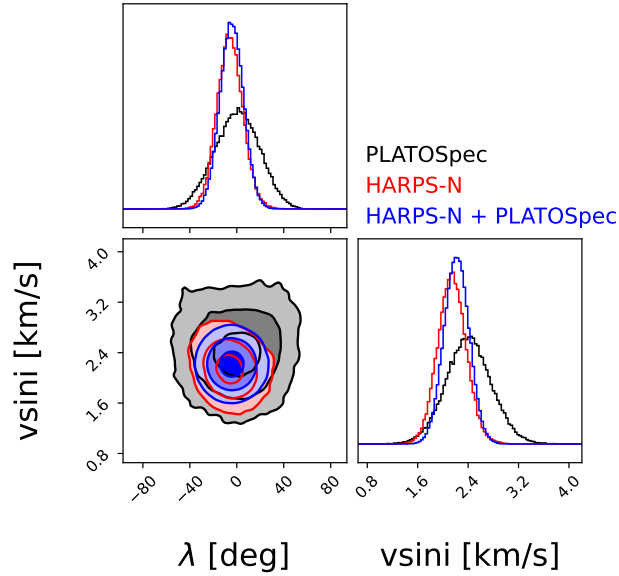


Fig. A2: Corner plot for WASP-35b showing posteriors for two parameters, projected spin-orbit angle λ and projected rotational velocity of the star $v \sin i_*$. The contours show 1, 2 and 3- σ deviations from the median. Data in red were obtained during a single transit with HARPS-N and presented in Zak et al. (2025a) while data in black are from two transits with the new PLATOSpec instrument. They show excellent agreement between the derived parameters. Data in blue are a joint fit of both datasets.

Table B.1: Radial velocity measurements for WASP-35.

Date	RV	RV uncertainty	Exp. time
[BJD _{TDB}]	[km s ⁻¹]	[km s ⁻¹]	[s]
2460681.55322686	17.7693	0.0201	1200
2460681.56718455	17.7438	0.0154	1200
2460681.58113067	17.7973	0.0143	1200
2460681.59508836	17.7496	0.0166	1200
2460681.60903448	17.7610	0.0187	1200
2460681.62299217	17.8007	0.0142	1200
2460681.63694986	17.7816	0.0143	1200
2460681.65089597	17.7837	0.0129	1200
2460681.66485365	17.7661	0.0123	1200
2460681.67881133	17.7161	0.0128	1200
2460681.69275744	17.7310	0.0121	1200
2460681.70671511	17.7228	0.0118	1200
2460681.72066122	17.7271	0.0124	1200
2460681.73461889	17.7260	0.0128	1200
2460681.74857656	17.7206	0.0138	1200
2460681.76252266	17.7189	0.0168	1200
2460681.77648033	17.7192	0.0185	1200
2460700.54737477	17.7445	0.0249	900
2460700.55784860	17.7750	0.0196	900
2460700.56927143	17.7741	0.0191	1020
2460700.58114562	17.7613	0.0183	1020
2460700.59301981	17.8035	0.0186	1020
2460700.60489400	17.8330	0.0180	1020
2460700.61677975	17.8120	0.0186	1020
2460700.62865394	17.7526	0.0181	1020
2460700.64052812	17.7671	0.0174	1020
2460700.65240231	17.7234	0.0173	1020
2460700.66427649	17.7457	0.0185	1020
2460700.67615067	17.6897	0.0176	1020
2460700.68802484	17.7330	0.0185	1020
2460700.69989902	17.6868	0.0190	1020
2460700.71177320	17.7541	0.0205	1020
2460700.72364738	17.7496	0.0216	1020
2460700.73552155	17.7778	0.0262	1020

Appendix B: Derived radial velocities

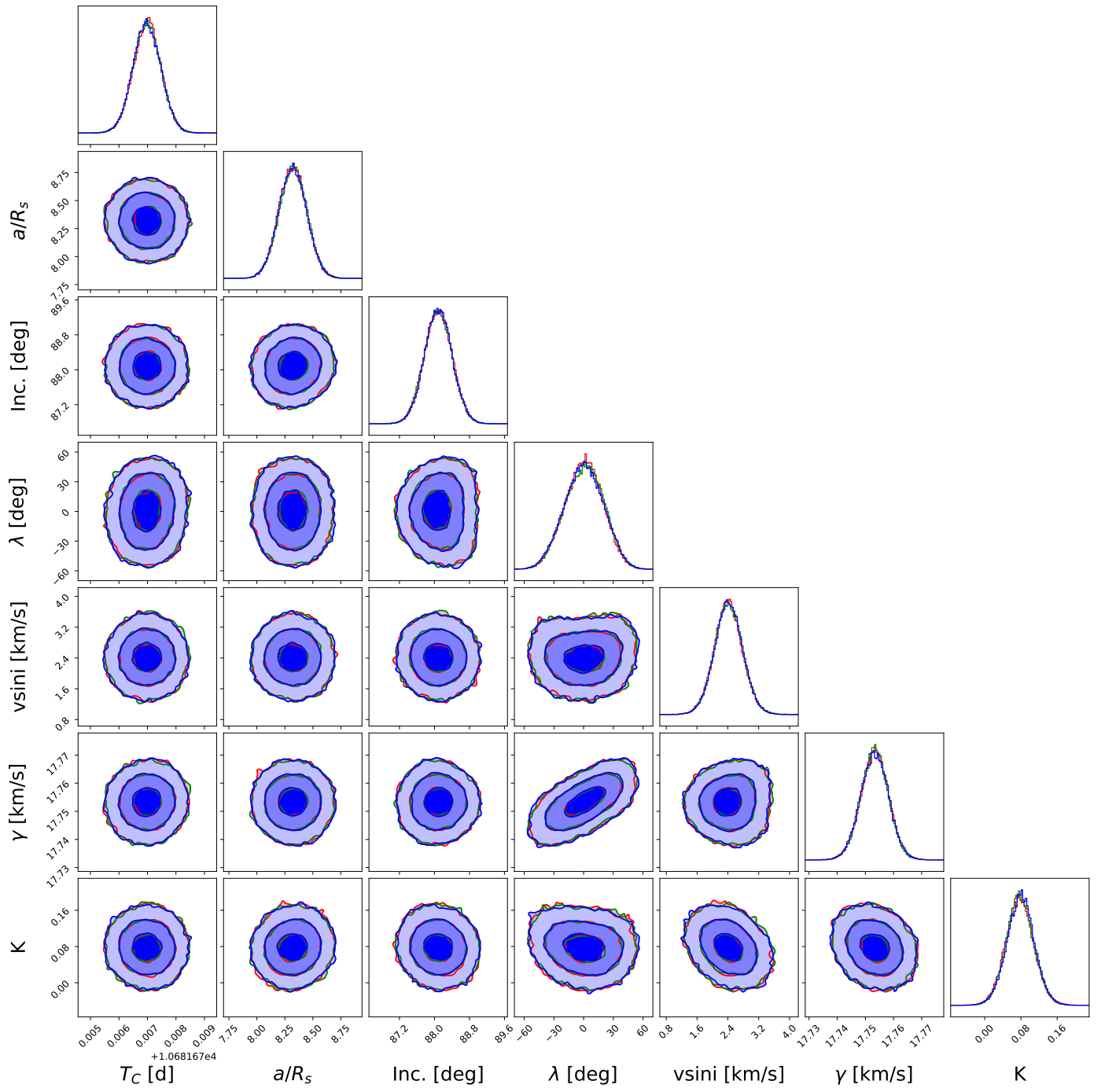


Fig. A3: MCMC results of WASP-35b. Three independent MCMC simulations are shown with different colors. The contours show 1, 2 and 3- σ deviations from the median.

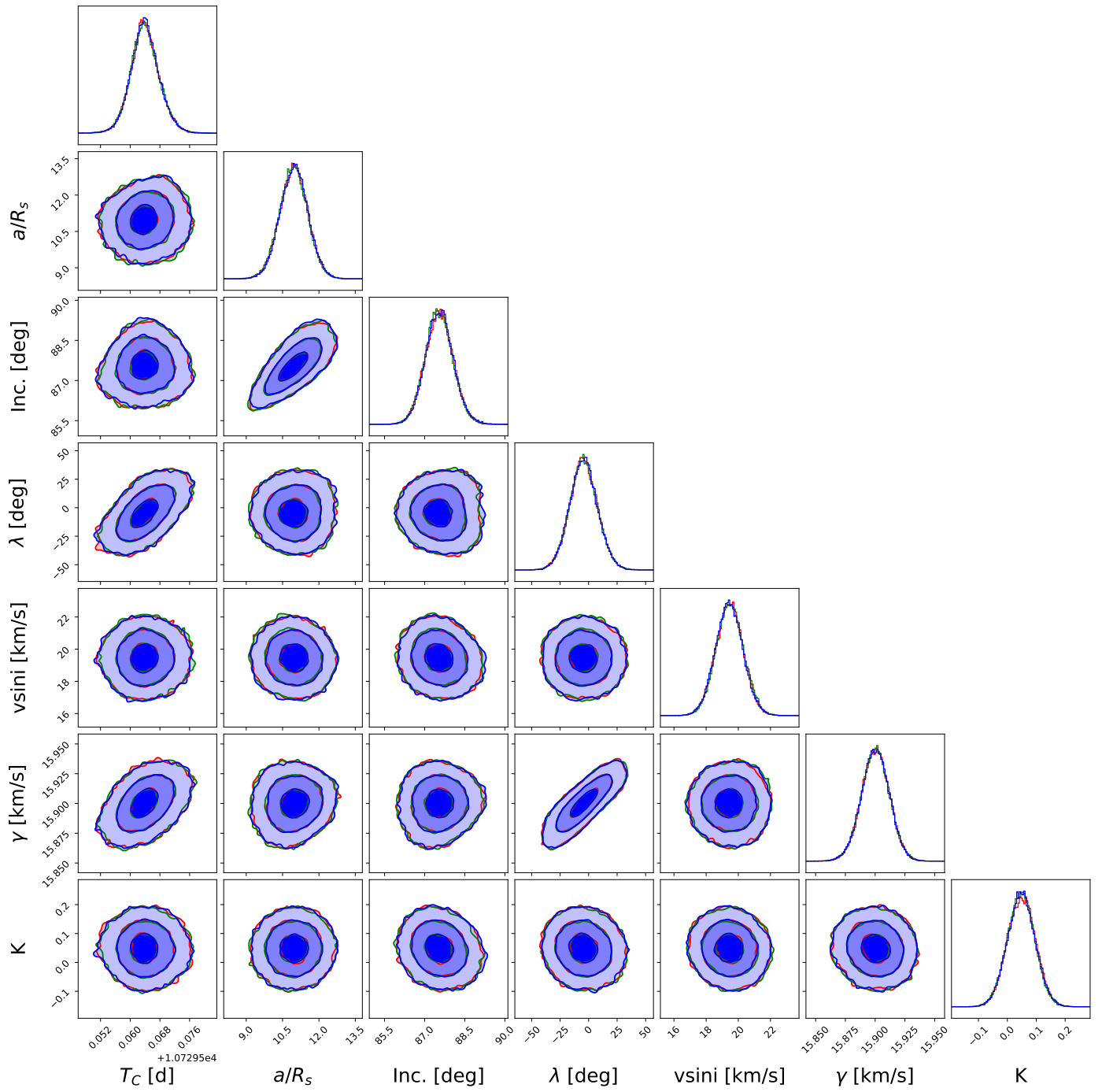


Fig. A4: MCMC results of TOI-622b. Three independent MCMC simulations are shown with different colors. The contours show 1, 2 and 3- σ deviations from the median.

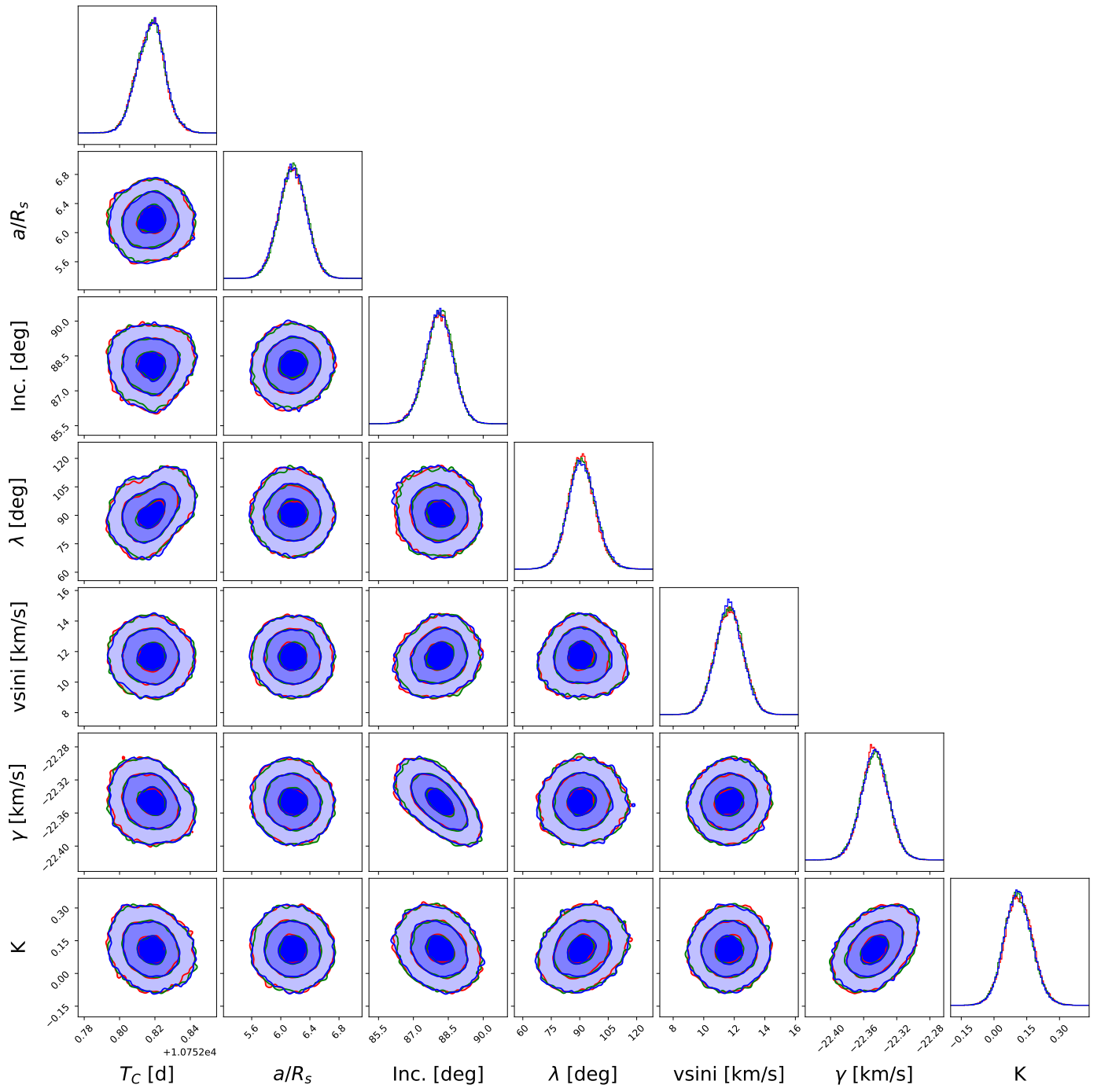


Fig. A5: MCMC results of K2-237b. Three independent MCMC simulations are shown with different colors. The contours show 1, 2 and 3- σ deviations from the median.

Table B.2: Radial velocity measurements for TOI-622.

Date [BJD _{TDB}]	RV [km s ⁻¹]	RV uncertainty [km s ⁻¹]	Exp. time [s]
2460716.76909215	15.8986	0.0316	900
2460716.77957833	15.8566	0.0304	900
2460716.79005294	15.8478	0.0284	900
2460716.80053913	15.8044	0.0298	900
2460716.81102531	15.8440	0.0314	900
2460716.82149992	15.8159	0.0317	900
2460716.83198610	15.8111	0.0325	900
2460716.84247228	15.8752	0.0305	900
2460716.85338670	15.8917	0.0299	900
2460716.86386131	15.8106	0.0317	900
2460716.87434749	15.7563	0.0320	900
2460793.48528093	15.9171	0.0316	900
2460793.49285585	15.8756	0.0331	900
2460793.49990417	15.9178	0.0299	900
2460793.50877532	15.9482	0.0245	900
2460793.51926099	15.9609	0.0246	900
2460793.52974667	16.0018	0.0239	900
2460793.54022076	16.0276	0.0234	900
2460793.55070643	15.9978	0.0239	900
2460793.56119210	15.9916	0.0263	900
2460793.57167777	15.9435	0.0252	900
2460793.58215187	15.9236	0.0242	900
2460793.59263754	15.8276	0.0241	900
2460793.60312320	15.8782	0.0242	900
2460793.61359730	15.8979	0.0243	900
2460793.62408296	15.8046	0.0243	900
2460793.63456863	15.8542	0.0252	900
2460793.64504272	15.8123	0.0258	900

Table B.3: Radial velocity measurements for K2-237.

Date [BJD _{TDB}]	RV [km s ⁻¹]	RV uncertainty [km s ⁻¹]	Exp. time [s]
2460752.74151981	-22.2392	0.0670	1200
2460752.75546794	-22.3986	0.0487	1200
2460752.77364103	-22.3856	0.0333	1750
2460752.79395552	-22.4809	0.0291	1750
2460752.81428159	-22.3529	0.0337	1750
2460752.83459609	-22.4147	0.0326	1750
2460752.85491058	-22.5531	0.0268	1750
2460752.87523664	-22.3925	0.0266	1750
2460752.89309718	-22.4353	0.0333	1300
2460752.90821439	-22.4511	0.0369	1300
2460787.65942431	-22.4138	0.0456	1600
2460787.67801357	-22.5013	0.0408	1600
2460787.69660284	-22.3185	0.0400	1600
2460787.71519210	-22.3788	0.0386	1600
2460787.73378136	-22.4204	0.0420	1600
2460787.75247479	-22.4254	0.0409	1600
2460787.77124925	-22.3107	0.0462	1600
2460787.79009315	-22.3039	0.0451	1600
2460787.80867082	-22.2765	0.0447	1600
2460787.82726007	-22.3319	0.0474	1600
2460787.84590719	-22.3789	0.0441	1600
2460787.86539927	-22.3262	0.0475	1600
2460800.68198632	-22.3043	0.0512	1200
2460800.69594538	-22.3384	0.0513	1200
2460800.70989287	-22.2357	0.0548	1200
2460800.72385194	-22.3942	0.0534	1200
2460800.73779942	-22.3015	0.0516	1200
2460800.75175848	-22.3724	0.0555	1200
2460800.76570597	-22.4482	0.0543	1200
2460800.77966502	-22.5075	0.0550	1200
2460800.79362408	-22.3671	0.0559	1200
2460800.80757156	-22.4988	0.0574	1200
2460800.82153061	-22.3526	0.0536	1200
2460800.83547808	-22.4352	0.0674	1200
2460800.84943713	-22.3298	0.0527	1200
2460800.86338460	-22.3894	0.0583	1200
2460800.87734365	-22.3674	0.0577	1200
2460800.89129112	-22.5943	0.0639	1200
2460800.90525016	-22.4263	0.0620	1200
2460800.91919762	-22.3268	0.0716	1200